

Cite this: *Soft Matter*, 2011, **7**, 10756

www.rsc.org/softmatter

PAPER

Systematic progressions of core-shell polygon containing tiling patterns in melts of 2nd generation dendritic miktoarm star copolymers

Jacob Judas Kain Kirkensgaard*

Received 14th June 2011, Accepted 9th August 2011

DOI: 10.1039/c1sm06115a

Dissipative particle dynamics simulations are used to investigate the self-assembly of generic 2nd generation dendritic 3-miktoarm star copolymers. These molecules can be conceptually conceived as the attachment of three ABC 3-miktoarm terpolymers to a common junction. In analogy to ABC 3-miktoarm star terpolymers the resulting morphologies show a number of cylindrical structures displaying a systematic progression through various 2D Archimedean tiling patterns as the molecular volume fractions are altered. The insertion of a variably sized junction region allows the controlled formation of tiling patterns where one polygonal component is a core-shell cylinder. A rich phase diagram is presented when invoking asymmetric interaction parameters indicating the possibility of jumping between these tiling patterns in a controllable way. We discuss how these core-shell containing tiling patterns potentially constitute self-assembled soft materials combining well-defined directional charge carriage and photonic band gap properties.

1 Introduction

One of the first examples of complex architecture multicomponent block copolymers was the ABC 3-miktoarm star terpolymers first synthesized almost two decades ago.^{1,2} A range of papers have since then reported the making of such macromolecules involving a number of different polymer species and synthesis techniques.^{3–14} One of the key features of ABC 3-miktoarm stars is the constraint imposed by the molecular star architecture which demands that the star junctions assemble along one-dimensional lines where the interfaces of each pair of polymer species meet.^{3,15} As a result of this constraint a number of structures can form in star shaped systems which are impossible to form in corresponding linear systems. For example, a number of cylindrical structures are both found experimentally and predicted from simulations which display 2D cross sections following various Archimedean tiling patterns,^{15–18} other complex cylindrical morphologies^{19,20} as well as quasi-crystalline patterns.^{21–23} Recently, equivalent structures are emerging in systems of smaller molecular weight ABC star molecules, both experimentally and theoretically^{24–27} illustrating that the formation of these patterns are generic and a fundamental consequence of the molecular architecture. In Fig. 1 the tiling patterns most commonly found in ABC 3-miktoarm star systems are illustrated and the notation employed to describe the tiling patterns are introduced. The tiling structures shown in Fig. 1 are believed to have a range of potential advanced material applications, particularly due to two properties. One is the line assembly of the

molecular junctions mentioned above, which in these systems is a guarantee of the formation of a nanofiber. This is considered an attractive functional feature with a range of potential applications such as molecular wires for nanosized ‘supramolecular electronics’.^{28,29} The other is the fact that several of these tiling patterns show photonic band gaps,^{30–34} *i.e.* they are photonic crystals, another highly sought property in contemporary material science. We will return to both these properties below.

A current trend in polymer chemistry is the conceptually appealing idea of ‘click’ chemistry or more generally, of a modular approach in the design of new molecules.^{35,36} The work presented here has been inspired by this modular idea as well as the continuing advances in recent years of the ability to synthesize ever more complex copolymer architectures.³⁷ We proceed along the modular design path well-knowing that the actual synthesis is in fact more involved and probably contains a range of polymeric techniques not classified as click chemistry

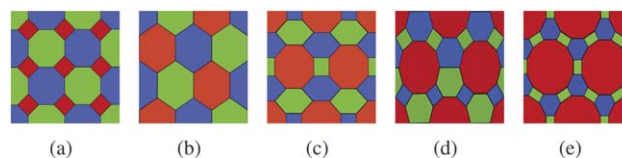


Fig. 1 Most commonly encountered tiling patterns in ABC star systems. (a) [8.8.4] (b) [6.6.6] (c) [8.6.4;8.6.6] (d) [10.6.4;10.6.6] (e) [12.6.4]. The tiling patterns are labeled by their Schläfli symbol¹⁵ that assigns a polygonal tiling pattern a set of numbers $[k_1, k_2, \dots, k_L]$ indicating that a vertex in the tiling is surrounded by a k_1 -gon, a k_2 -gon, ... in cyclic order. Tilings with more than one topologically distinct vertex are denoted $[k_1, k_2, k_3; k_4, k_5, k_6]$.

Department of Basic Sciences and Environment, Faculty of Life Sciences, University of Copenhagen, Denmark. E-mail: kirkensgaard@life.ku.dk

per se. Nevertheless, in Fig. 2(a) a modular approach to the making of ABC 3-miktoarm stars is shown where three single polymer chains are clicked onto a common junction. Extending this idea another step one can imagine clicking three ABC miktoarm stars onto another common junction thus creating a 2nd generation dendritic miktoarm star terpolymer. Well-defined examples of such molecules has recently been synthesized,^{38,39} however no report has yet been made of their bulk self-assembly properties. In this study we employ coarse grained computer simulations to investigate possible mesostructural self-assembly morphologies of these new complex molecular architectures.

2 Simulations and modeling

The self-assembly of the 2nd generation dendritic miktoarm stars is explored using dissipative particle dynamics (DPD) simulations following the implementation described previously.⁴⁰ Specific details about employed parameters are the following: The interactions between any two different polymer species i and j separated by a distance r_{ij} are described by the soft potential

$$V^C(r_{ij}) = \begin{cases} \frac{a_{ij}}{2} \left(1 - \frac{r_{ij}}{r_c}\right)^2 & \text{for } r_{ij} \leq r_c \\ 0 & \text{for } r_{ij} > r_c \end{cases} \quad (1)$$

with $r_c = 1$ and beads are connected with harmonic bonds *via* the potential

$$V^S = \frac{C}{2}(r_{ij} - r_0)^2 \quad (2)$$

with $r_0 = 0$ and $C = 4$. The integration of the equations of motion is done using a standard velocity-Verlet algorithm with time step $\Delta t = 0.02$ and $k_B T = 1$. All simulations are performed in a cubic box of volume L^3 and with particle density $\rho = 3$. The box side lengths vary between $L = 18$ – 23 and for all structures different box sizes has been checked to eliminate finite size effects.⁴⁰ At a density of $\rho = 3$ the interaction parameter between unlike particles can be related to the Flory-Huggins interaction parameter χ_{ij} ⁴¹ so that

$$a_{ij} = a_{ii} + 3.497 \chi_{ij} \quad (3)$$

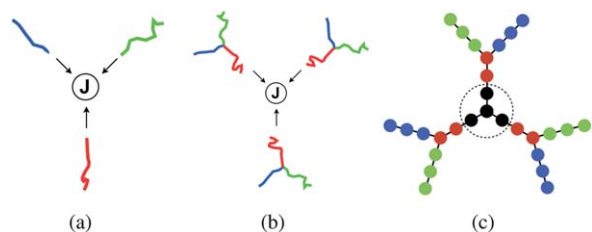


Fig. 2 Modular approach to miktoarm copolymer synthesis and molecular simulation topology. (a) Making an ABC 3-miktoarm terpolymer by clicking 3 linear polymer chains onto a common junction. (b) Making a 2nd generation dendritic miktoarm terpolymer by clicking 3 ABC 3-miktoarm stars onto a common junction. (c) An example of a model 2nd generation dendritic miktoarm star. This is labeled $(n_L, n_A, n_B, n_C) = (1,2,3,3)$ indicating the number of beads of each color, not counting the central junction bead. Color code: L: black, A: red, B: blue, C: green.

with the like-like interaction parameter determined from the compressibility of water to be $a_{ii} = 25$.⁴¹ Here we take a purely qualitative approach exploring generic traits due to symmetric and asymmetric interactions and do not intend to match any specific polymer system. Simulations were run using the ESPResSo package⁴² within the framework developed earlier to simulate branched molecules in general.²⁴ Simulation snapshots were all made with the VMD package.⁴³

In Fig. 2(c) we illustrate the topology and our nomenclature for the model molecules. Each 2nd generation dendritic miktoarm star consists of three ABC 3-miktoarm stars attached to a common junction. The 3-miktoarm stars are made from n_A , n_B and n_C beads of color red, blue and green respectively and are connected to the black junction region at the end of the red chain. We will use this color code throughout the manuscript. The junction region marked by the dashed circle in Fig. 2(c) always has a central bead and can also contain a linker with n_L beads between this central bead and the red arm of the attached 3-miktoarm star. Using the short notation (n_L, n_A, n_B, n_C) the example in Fig. 2(c) thus represents a (1,2,3,3) 2nd generation dendritic miktoarm star. In this study we constrain ourselves to stars with $n_B = n_C$. To quantify the relative volume fractions in the system we define the number x as the ratio between the number of beads in one of the two outer chains and the number of beads between the junction up to the branch point, *i.e.*

$$x = \frac{n_L + n_A}{n_B} \quad (4)$$

Thus, the molecule illustrated in Fig. 2(c) represents a $x = 1$ molecule. We will plot our results as a function of x in the following.

3 Results and discussion

3.1 Symmetric interactions

We initially assume symmetric interaction parameters between different polymer species and employ $a_{ij} = 45$. In Fig. 3 a series of simulations for $x = 1$ are shown but varying n_L and n_A . All structures are following the [6.6.6] tiling showing that it is the overall volume fraction represented by the $n_L + n_A$ inner star beads that determine the resulting tiling pattern. This justifies the definition of x which then also roughly coincides with the definition employed in previous work on ABC miktoarm stars¹⁵ where a similar parameter described the volume fraction of one arm compared to the other two having equal size in analogy to us having $n_B = n_C$ here. The difference is then the central connecting bead joining triplets of ABC stars in our case, *i.e.* the molecular architecture. Below we will compare our results with results from regular ABC stars. Returning to the results in Fig. 3 we see that within the [6.6.6] tiling pattern the alteration of the size of the junction region simply transforms this particular polygonal domain into a core-shell structure as a simple consequence of the molecular architecture.

In the following we will set $n_L = 1$, *i.e.* fix the junction region size and then vary x by altering the values of n_A and $n_B = n_C$. The results are visually summarized in Fig. 4 and simulation details are listed in Table 1. In Fig. 4, results from two previous studies on ABC miktoarm stars are also shown for comparison, one is

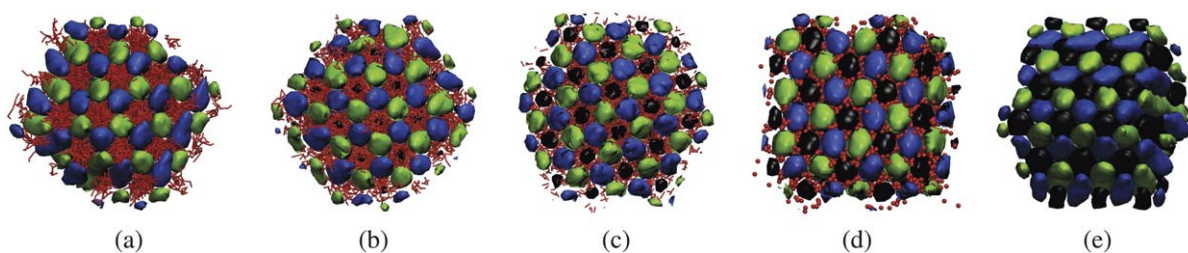


Fig. 3 Varying the ratio between n_A and n_L keeping $x = 1$ and employing symmetric interactions with $a_{ij} = 45$. All resulting patterns follow the [6.6.6] tiling while altering the composition of the core-shell domain. Junction is always black unless specified, and specific (n_L, n_A, n_B, n_C) values are (a) (0,3,3,3) with red junction, (b) (0,3,3,3), (c) (1,2,3,3), (d) (2,1,3,3) and (e) (3,0,3,3).

based on self-consistent field theory⁴⁴ and the other on Monte Carlo simulations.¹⁵ As can be seen these two studies are in reasonable agreement on the predicted morphologies as a function of x . Two notable differences are the question of whether the low x lamellar phase distributes the minority component evenly over the interface (denoted [LAM₃]) or as spheres (denoted [L + S]) and the almost complete absence of the [12.6.4] tiling in the Monte Carlo study. We will return to the latter below.

As can be seen in Fig. 4 the 2nd generation dendritic miktoarm stars largely follow the same behavior. At low x a lamellar structure is formed with the minority components distributed evenly on the interface, *i.e.* a [LAM₃] structure. Over a narrow x -interval the system then goes from the lamellar through two different perforated lamellae structures into a region of cylindrical structures systematically following a progression of tiling patterns described below. We note that the transformation from lamellar to cylindrical structures through perforated lamellae, or *mesh* phases, is expected from theoretical considerations.⁴⁵ The first perforated lamellae structure [PL] found at $x = 0.37$ has a number of globular junction domains embedded inside the green and blue domains respectively. This is in contrast to the second perforated lamellae structure found at $x = 0.43$ where the junction region forms cylinders and where the morphology is locally arranged in a [8.8.4] tiling as shown in the figure. Thus, we

Table 1 Simulation details for results presented in Fig. 4 invoking symmetric interaction parameters between all pairs of unlike particle species, $a_{ij} = 45$. The columns contain the number of beads in each arm of each color, the ratio x defined in eqn (4) and the morphology found for each molecule

n_L	n_A	$n_B = n_C$	x	Morphology
1	0	3	0.33	[LAM ₃]
1	2	8	0.37	[PL]
1	2	7	0.43	[PL-8.8.4]
1	2	6	0.5	[8.8.4]
1	2	5	0.60	[8.8.4]
1	1	3	0.66	[8.8.4]
1	2	4	0.75	[8.8.4]
1	2	3	1	[6.6.6]
1	3	3	1.33	[6.6.6]
1	4	3	1.66	[8.6.4;8.6.6]
1	5	3	2	[8.6.4;8.6.6]
1	6	3	2.33	[10.6.4;10.6.6]
1	4	2	2.5	[10.6.4;10.6.6]
1	5	2	3	[10.6.4;10.6.6]
1	6	2	3.5	[NET]
1	7	2	4	[NET]
1	8	2	4.5	[NET]
1	9	2	5	[NET]

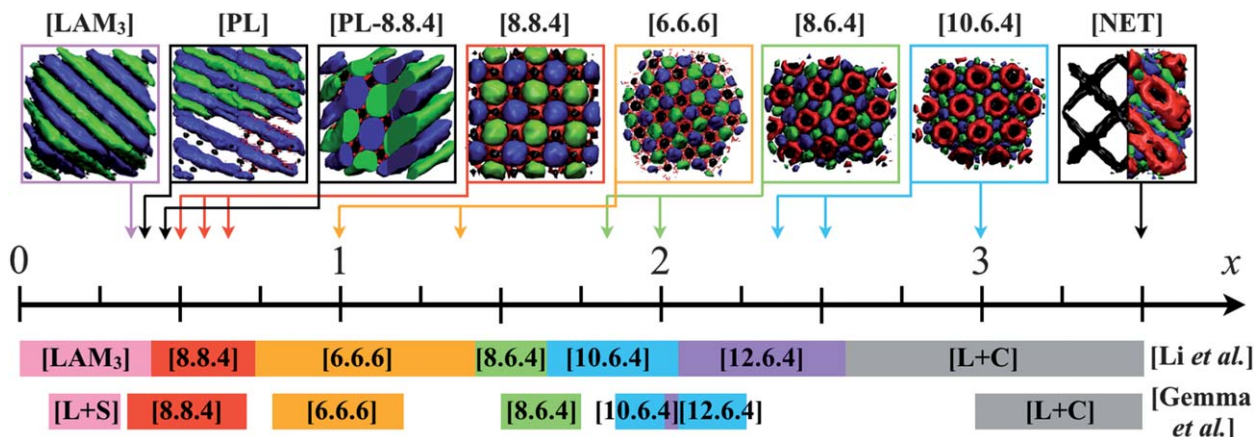


Fig. 4 Varying the composition by varying x with symmetric interaction parameters $a_{ij} = 45$. As x changes the system follows a systematic progression through different tiling patterns. The phase progression is $x = 0.33 \rightarrow$ [LAM₃], $x = 0.37 \rightarrow$ [PL], $x = 0.43 \rightarrow$ [PL-8.8.4], $x = 0.5-0.75 \rightarrow$ [8.8.4], $x = 1-1.33 \rightarrow$ [6.6.6], $x = 1.66-2 \rightarrow$ [8.6.4;8.6.6], $x = 2.33-3 \rightarrow$ [10.6.4;10.6.6] and for $x > 3 \rightarrow$ [NET] denoting unidentified network structures as outlined in the text. Below the x -axis the results from previous work on ABC 3-miktoarm stars are shown for comparison. Top row is based on self-consistent field theory calculations by Li *et al.*⁴⁴ and the bottom row is based on the Monte Carlo simulations done by Gemma *et al.*¹⁵

are right on the phase border to the tiling patterns where the [8.8.4] tiling is the first to appear. The region of tiling patterns extends from x values between 0.5 and 3. In this region, the polygonal composition changes systematically with the relative volume fractions in the system in complete qualitative agreement with previous simulation and theoretical work on ABC stars.^{15,26,44,46} We see that as x increases, the morphologies adopt the phase sequence [8.8.4] \rightarrow [6.6.6] \rightarrow [8.6.4;8.6.6] \rightarrow [10.6.4;10.6.6] with the core-shell domain occupying progressively larger polygonal domains. The agreement with the work on ABC stars as shown in Fig. 4 is only qualitative. For larger values of x the phase positions of the tiling patterns are shifted upwards compared to the regular ABC stars which we consider a result of the molecular architecture. This is because for any value of x , the naturally induced curvature of the 2nd generation dendritic miktoarm stars is higher than that of the corresponding ABC miktoarm star due to the dendritic nature of the molecules and the added surface tension between the 'core' and the 'shell'. Effectively this will stabilize a tiling pattern with a lower polygonal composition compared to the ABC star of matching composition. Another issue is the fact that we do not find the [12.6.4] tiling in this simulation series, in somewhat agreement with the Monte Carlo simulations by Gemma *et al.* where this is only found in one case.¹⁵ This is probably due to the fact that all these results are obtained under the assumption that two components occupy the exact same volume fraction. As can be seen in Fig. 1 the [12.6.4] tiling is the only one that does not have permutation symmetry of the green and blue components. This means that it is impossible to make a [12.6.4] tiling where the two minority components occupy exactly the same volume without inducing some degree of packing frustration in the idealized setting of complete symmetry of these two components. On the contrary, when the constraints of interaction and volume fraction symmetry is lifted we would expect the [12.6.4] tiling pattern to form readily under the right conditions which is also found to be the case as shown below and in the Monte Carlo study.¹⁵ The fact that Li *et al.*⁴⁴ does predict the [12.6.4] tiling even under this constraint lies in the methodical procedures relevant for the field theory calculations where the various structures are postulated and then used as initial conditions for the calculations. This is contrary to our method and that of Gemma *et al.*¹⁵ where the system evolves from a random state. Judging from the very small free energy differences shown in Li *et al.*⁴⁴ the suggested phase window of the [12.6.4] tiling can certainly be questioned. For $3 < x < 5$ the 2nd generation dendritic miktoarm stars form a number of core-shell network phases denoted [NET] in Fig. 4. The exact nature of these network structures has not been determined, but they are not any of the ones usually found in soft matter systems like the P, D and G bicontinuous structures. The ones found so far typically form 3-connected nets with 2 core-shell nets of black/red intertwined and separated by a wall of segregated blue/green minority components. These potentially new network structures will be the topic of future work. We note that it is a general problem to reliably establish three-periodic equilibrium structures in these type of simulations using cubic boxes with periodic boundary conditions.⁴⁰ This is usually not a concern for structures of one- or two-dimensional periodicity like the tiling patterns described here since these can effectively reorient in the box to match the boundary conditions.

3.2 Asymmetric interactions

A more realistic scenario is that the interaction parameters are not symmetric. Here we investigate a situation commonly encountered in block copolymer systems, namely that one of the pairwise interaction parameters is different from the others. We present two specific scenarios in the following, one where a_{AB} is varied while all other interaction parameters are kept equal and set to $a_{ij} = 45$ and likewise a scenario where a_{BC} is varied. To ensure this investigation remains computationally feasible we limit ourselves to four x -values each representing one of the tiling patterns found using only symmetric interactions. The results are summarized in Fig. 5 as a combined $x - a_{AB}$ and $x - a_{BC}$ phase diagram with snapshots of the additional morphologies found shown in Fig. 6. Note that in both scenarios in Fig. 5, the line at $a_{AB} = a_{BC} = 45$ represents the same simulations as that shown in Fig. 4, *i.e.* invoking symmetric interactions between all different particle species. In Fig. 5 we see that varying the interaction parameters results in a rich phase behavior for both scenarios. Starting with the variation of a_{AB} , we see that for both $x = 2/3$ and $x = 1$ the underlying tilings largely remain as [8.8.4] and [6.6.6] respectively. The exception is for $a_{AB} < 35$ and $x = 1$ where

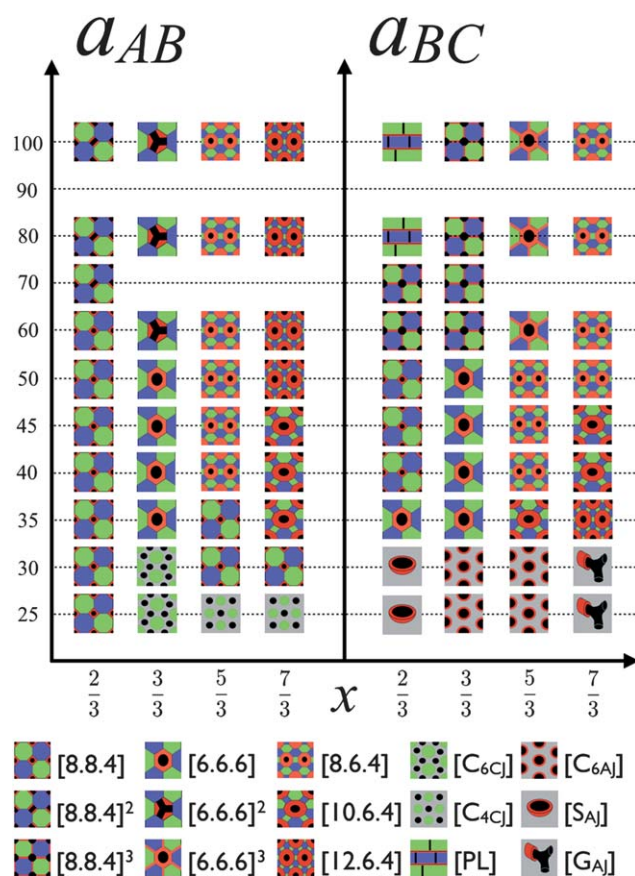


Fig. 5 Phase diagrams for two scenarios of asymmetric interaction parameters investigated at 4 representative values of x . (Top left) Varying a_{AB} with all other pair interactions $a_{ij} = 45$. (Top right) Varying a_{BC} with all other pair interactions $a_{ij} = 45$. (Bottom) Legend describing the symbols used above representing the different morphologies shown in Fig. 6. Gray colour represents a mixed domain of two colors, either A/B (red/blue) or B/C (blue/green).

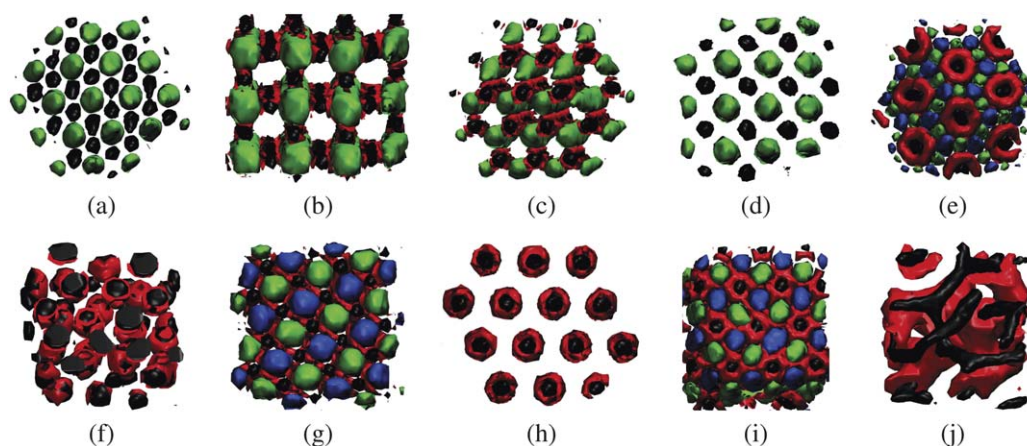


Fig. 6 Individual simulation images of the phases presented in the phase diagram in Fig. 5 which have not been shown previously in Fig. 4. In some images one or two components are omitted for clarity. (a) $[C_{6CJ}]$ (b) $[8.8.4]^2$ (c) $[6.6.6]^2$ (d) $[C_{4CJ}]$ (e) $[12.6.4]$ (f) $[S_{AJ}]$ (g) $[8.8.4]^3$ (h) $[C_{6AJ}]$ (i) $[6.6.6]^3$ (j) $[G_{AJ}]$.

the A and B components mix and a cylindrical structure is formed with hexagonally arranged rods of green and black (denoted $[C_{6CJ}]$, see Fig. 6(a)). Interestingly, even for complete miscibility of the A and B components, the structure remains in the $[8.8.4]$ tiling for $x = 2/3$ although the structure appears more fuzzy than at higher a_{AB} values. Although the underlying tilings are the same for higher a_{AB} values, the structure changes to accommodate the increased A–B surface tension. This is reflected in the behavior of the black junction domain which arranges so as to minimize the A–B surface area thus disrupting the central core-shell structure as seen for $a_{AB} > 60$ and $a_{AB} > 50$ for $x = 2/3$ and $x = 1$ respectively. The resulting structures are shown in Fig. 6(b–c) and denoted $[8.8.4]^2$ and $[6.6.6]^2$ respectively. In both the latter figures the blue component is omitted and the red domains can be seen to preferably share an interface with the green component. For $x = 5/3$ and $x = 7/3$ we again find cylindrical phases for $a_{AB} = 25$, but now the rods of green and black are arranged tetragonally (denoted $[C_{4CJ}]$, see Fig. 6(d)). Increasing a_{AB} for both these x -values we find phase progressions that go through a $[8.8.4]$ tiling into tilings of higher polygonal composition. For $x = 5/3$ the phase progression is $[C_{4CJ}] \rightarrow [8.8.4] \rightarrow [8.6.4; 8.6.6]$ and for $x = 7/3$ it is $[C_{4CJ}] \rightarrow [8.8.4] \rightarrow [10.6.4; 10.6.6] \rightarrow [12.6.4]$. The latter structure is shown in Fig. 6(e). As discussed above, the $[12.6.4]$ tiling is easily found when the constraint of complete symmetry between the B and C components is lifted, even though it here is indirectly through the asymmetry of the AB vs. AC interactions respectively.

In the right part of Fig. 5 the effects of varying a_{BC} are shown for the 4 chosen values of x . Starting with $x = 2/3$ the B and C components mix for $a_{BC} < 35$ and the system makes a core-shell sphere packing of globular junction domains wrapped in the A component (denoted $[S_{AJ}]$, see Fig. 6(f)). At $a_{BC} \geq 35$ the different domains segregate and goes through a $[6.6.6]$ tiling at $a_{BC} = 35$ into a region of $[8.8.4]$ tilings. For $40 \geq a_{BC} \leq 50$ this is a regular $[8.8.4]$ tiling, but for $a_{BC} > 50$ the system again adapts to the increased surface tension by minimizing the BC surface area through the insertion of red A component between the B and C domains. This structure, denoted $[8.8.4]^3$, is shown in Fig. 6(g). For even higher values of a_{BC} we again find a perforated lamellae

structure like [PL] illustrated above in Fig. 4. For $x = 1$ the phase progression consists of 3 structures: a core-shell cylinder phase denoted $[C_{6AJ}]$ for $a_{BC} \leq 30$ shown in Fig. 6(h), a $[6.6.6]$ tiling for $35 \geq a_{BC} \leq 50$ and finally the $[8.8.4]^3$ structure for $a_{BC} > 50$ again reflecting interfacial area minimization between the B and C components. For $x = 5/3$ we again find the $[C_{6AJ}]$ structure for low a_{BC} followed by $[10.6.4; 10.6.6]$ at $a_{BC} = 35$ and $[8.6.4; 8.6.6]$ for $40 \geq a_{BC} \leq 50$. For $a_{BC} > 50$ a new structure appears denoted $[6.6.6]^3$. Again the red component minimizes the B–C interface analogue to the $[8.8.4]^3$ structure, but now overlaying a $[6.6.6]$ tiling, see Fig. 6(i). Finally, at $x = 7/3$ we find for $a_{BC} < 35$ a core-shell gyroid structure with the junction region wrapped in red A embedded in a matrix of mixed B and C. This is denoted $[G_{AJ}]$ and is shown in Fig. 6(j). For larger values of a_{BC} we find the phase progression $[12.6.4]$ (at $a_{BC} = 35$) $\rightarrow [10.6.4; 10.6.6] \rightarrow [8.6.4; 8.6.6]$.

Comparing the two phase diagrams in Fig. 5 a general trend appears. One can relate the changes in interaction parameters to an ‘effective x ’ value so that raising a_{AB} and a_{BC} corresponds to raising and lowering the effective x -value respectively. This can be seen for all values of x , but most clearly by looking at $x = 7/3$ where we see that raising the two interaction parameters results in the phase progressions $[8.8.4] \rightarrow [10.6.4; 10.6.6] \rightarrow [12.6.4]$ for a_{AB} and $[12.6.4] \rightarrow [10.6.4; 10.6.6] \rightarrow [8.6.4; 8.6.6]$ for a_{BC} . In both cases, the phase changes induced by the altered interaction parameters indicates that by proper design and depending on chemical characteristics, these structures can be controlled by external stimuli, the immediately most relevant being temperature.

4 Discussion

One of the current interests in material science regards self-assembled charge carrying cylindrical structures where the intra- and intercolumnar organization is well defined, stable and can be precisely controlled. One example is columnar structures formed from discotic polycyclic aromatic hydrocarbons where desired macroscopic properties like solubility, liquid crystal formation and high charge carrier rates are tuned by manipulating the

periphery of various π -conjugated molecular cores.⁴⁷ Along with a range of other π -conjugated systems, these types of molecules are key constituents in a contemporary quest for 'supramolecular electronics', *i.e.* wires of electronic components in the nanometre range, in between molecular (Ångstrom scaled) and plastic (micrometre scaled) electronics.^{28,29} As already mentioned in the introduction, supramolecular electronics is foreseen to influence a number of potential applications on the nanoscale, for example photovoltaic devices, light-emitting diodes, logic gates and field effect transistors. Although the junction region as it has been represented in the simulations here does not model π -conjugated cores directly, one might expect that it would be this type of charge carrier unit which would be used in these systems. However, the generic nature of the simulations presented here illustrates that the exact characteristics of the junction region will not be crucial as long as the dimensions of the junction remains relatively small compared to the other components. Comparing typical sizes of the molecular cores mentioned above⁴⁷ (<5 nm diameters) to the size of the individual polymer chains making the 2nd generation dendritic miktoarm star terpolymers synthesized recently^{38,39} where each chain has a radius of gyration at least 3 times the core diameters this criteria will usually be met. In fact, the π -conjugated cores themselves will likely favor these cylindrical structures due to attractive core-core interactions. As mentioned in the introduction some of the tiling patterns described here show photonic band gaps.³⁰ Further, it has been shown with ABC 3-miktoarm star terpolymers that it is possible to push the lattice parameters of these structures into the regime of visible light.²³ Thus, a possible application of the structures presented here would be as self-assembled materials with combined charge transport and photonic band gap properties. To the knowledge of the author this constitutes a new combination of properties in soft material science. Of the tiling patterns investigated theoretically in terms of photonic band gaps³⁰ we find 3 in this work, the Archimedean tilings [8.8.4], [6.6.6] and [12.6.4]. Particularly the latter is interesting as this structure shows complete photonic band gaps. Another tiling of interest with promising photonic properties is the [3.3.4.3.4] Archimedean tiling which is an approximant to a dodecagonal quasicrystal, both of which have been found experimentally in blends of regular ABC 3-miktoarm stars and homopolymers of one of the star components.²² Although, we have not found these structures in this study there is no reason why they would not appear in this system by suitable tuning of the composition, for example by lifting the constraint of $n_B = n_C$.

A final note concerns the relation between the molecules investigated here and regular dendrimers^{48,49} and dendronized polymers. One of the key features of dendrimers is the precise structural control obtained during the synthesis originating from the sequential procedure. This means that a number of structural characteristics such as number of surface groups, size and molecular weight can be predicted theoretically solely from knowledge of the generation and the core and branch cell multiplicities.⁴⁸ As predicted by de Gennes and Hervet steric effects come into play at higher generations restricting the ideal growth of the dendrimer.⁵⁰ However, the generation limit of this to occur is dependent on the length between branch points such that longer spacer chains allow a higher generation to be realized. Thus, the polymeric nature of the molecules discussed here should

allow higher dendritic generations to be realized if a suitable synthesis strategy can be made. In topological terms, a regular dendrimer is a special case of the molecules investigated here only with polymer species $A = B = C$. In fact, a number of examples have been synthesized of topologically equivalent molecules to the ones investigated here, but only consisting of one or two distinct polymer species.⁵¹⁻⁵⁵ The interplay between core and branching multiplicity, generation and overall design of higher generation multicomponent dendritic miktoarm stars is generally awaiting to be explored further which also applies to the behavior of these molecules in selective solvents. A significant portion of the work on dendrimers, dendrons and dendronized polymers concerns their solution self-assembly where a number of interesting structures have been found or predicted, for example various micellar structures,^{56,57} advanced micellar and columnar structures⁵⁸⁻⁶⁰ and helical network formation.⁶¹⁻⁶³ As has been shown here, 2nd generation dendritic 3-miktoarm star copolymers potentially form a range of interesting structures in bulk and it should be anticipated that this is also the case in solution, the exploration of which will be the topic of future work.

5 Conclusions

Dissipative particle dynamics simulations of generic 2nd generation dendritic 3-miktoarm star copolymers have been presented. The simulations show that invoking symmetric interactions between all components a systematic progression through cylindrical structures with 2D cross sections following various tiling patterns are found. This behavior is consistent with previous work on ABC 3-miktoarm terpolymers. Investigating two scenarios of asymmetric interactions a rich phase diagram appears indicating a number of opportunities to switch between various tiling patterns in a controlled way. The potential use of 2nd generation dendritic 3-miktoarm star copolymers in advanced nano-materials have been discussed, particularly the potential to act as novel self-assembled materials combining directional charge carriage and photonic crystal properties.

Acknowledgements

Parts of this research were undertaken at the NCI National Facility in Canberra, Australia, which is supported by the Australian Commonwealth Government. Financial support from The Lundbeck Foundation is gratefully acknowledged.

References

- 1 H. Iatrou and N. Hadjichristidis, *Macromolecules*, 1992, 4649.
- 2 T. Fujimoto, H. Zhang, T. Kazama, Y. Isono, H. Hasegawa and T. Hashimoto, *Polymer*, 1992, 33, 2208.
- 3 S. Sioula, N. Hadjichristidis and E. Thomas, *Macromolecules*, 1998, 31, 8429–8432.
- 4 S. Sioula, N. Hadjichristidis and E. Thomas, *Macromolecules*, 1998, 31, 5272–5277.
- 5 H. Huckstadt, V. Abetz and R. Stadler, *Macromol. Rapid Commun.*, 1996, 17, 599–606.
- 6 O. Lambert, S. Reytenauer, G. Hurtrez, G. Riess and P. Dumas, *Polym. Bull.*, 1998, 40, 143–149.
- 7 V. Bellas, H. Iatrou and N. Hadjichristidis, *Macromolecules*, 2000, 33, 6993.
- 8 A. Hirao, M. Hayashi and N. Haraguchi, *Macromol. Rapid Commun.*, 2000, 21, 1171–84.

- 9 A. Hirao, Y. Tokuda, K. Morifuji and M. Hayashi, *Macromol. Chem. Phys.*, 2001, **202**, 1606–1613.
- 10 A. Zioga, S. Sioula and N. Hadjichristidis, *Macromol. Symp.*, 2000, **157**, 239–249.
- 11 X. Feng and C. Pan, *Macromolecules*, 2002, **35**, 4888–93.
- 12 C. Celik, G. Hizal and U. Tunca, *J. Polym. Sci., Part A: Polym. Chem.*, 2003, **41**, 2542–8.
- 13 M. Nasser-Eddine, S. Reutenauer, C. Delaite, G. Hutrez and P. Dumas, *J. Polym. Sci., Part A: Polym. Chem.*, 2004, **42**, 1745–1751.
- 14 N. Hadjichristidis, H. Iatrou, M. Pitsikalis, S. Pispas and A. Avgeropoulos, *Prog. Polym. Sci.*, 2005, **30**, 725–782.
- 15 T. Gemma, A. Hatano and T. Dotera, *Macromolecules*, 2002, **35**, 3225–3227.
- 16 A. Takano, S. Wada, S. Sato, T. Araki, K. Hirahara, T. Kazama, S. Kawahara, Y. Isono, A. Ohno, N. Tanaka and Y. Matsushita, *Macromolecules*, 2004, **37**, 9941–9946.
- 17 A. Takano, W. Kawashima, S. Wada, K. Hayashida, S. Sato, S. Kawahara, Y. Isono, M. Makihara, N. Tanaka, D. Kawaguchi and Y. Matsushita, *J. Polym. Sci., Part B: Polym. Phys.*, 2007, **45**, 2277–2283.
- 18 K. Hayashida, W. Kawashima, A. Takano, Y. Shinohara, Y. Amemiya, Y. Nozue and Y. Matsushita, *Macromolecules*, 2006, **39**, 4869–4872.
- 19 K. Hayashida, N. Saito, S. Arai, A. Takano, N. Tanaka and Y. Matsushita, *Macromolecules*, 2007, **40**, 3695–3699.
- 20 K. Yamauchi, K. Takahashi, H. Hasegawa, H. Iatrou, N. Hadjichristidis, T. Kaneko, Y. Nishikawa, H. Jinnai, T. Matsui, H. Nishioka, M. Shimizu and H. Fukukawa, *Macromolecules*, 2003, **36**, 6962–6966.
- 21 T. Dotera and T. Gemma, *Philos. Mag.*, 2006, **86**, 1085–109.
- 22 K. Hayashida, T. Dotera, A. Takano and Y. Matsushita, *Phys. Rev. Lett.*, 2007, **98**, 195502.
- 23 A. Takano, W. Kawashima, A. Noro, Y. Isono, N. Tanaka, T. Dotera and Y. Matsushita, *J. Polym. Sci., Part B: Polym. Phys.*, 2005, **43**, 2427–2432.
- 24 J. J. K. Kirkensgaard and S. Hyde, *Phys. Chem. Chem. Phys.*, 2009, **11**, 2016–2022.
- 25 S. T. Hyde, L. de Campo and C. Oguey, *Soft Matter*, 2009, **5**, 2782–2794.
- 26 J. J. K. Kirkensgaard and S. Hyde, In preparation.
- 27 L. de Campo, T. Varslot, M. Moghaddam, J. Kirkensgaard, K. Mortensen and S. Hyde, *Phys. Chem. Chem. Phys.*, 2011, **13**, 3139–3152.
- 28 F. Hoeben, P. Jonkheijm, E. W. Meijer and A. Schenning, *Chem. Rev.*, 2005, **105**, 1491–1546.
- 29 A. Schenning and E. Meijer, *Chem. Commun.*, 2005, 3245–3258.
- 30 K. Ueda, T. Dotera and T. Gemma, *Phys. Rev. B: Condens. Matter Mater. Phys.*, 2007, **75**, 195122.
- 31 J.-Y. Chen, Y.-G. Li, J.-Y. Yeh, L.-W. Chen and C.-C. Wang, *J. Optoelectron. Adv. Mater.*, 2009, **11**, 197–203.
- 32 D. Jovanovic, R. Gajic and K. Hingerl, *Opt. Express*, 2008, **16**, 4048–4058.
- 33 D. Jovanovic, R. Gajic and K. Hingerl, *Acta Phys. Polon. A*, 2009, **116**, 642–644.
- 34 Z. Qi, H. Kui, S. Xiao-Peng, T. Xing, W. Qiong-Hua, L. Ming-Xue and W. Yu-Xi, *Acta Phys. Sinica*, 2010, **59**, 7060–7065.
- 35 H. Kolb, M. Finn and K. Sharpless, *Angew. Chem., Int. Ed.*, 2001, **40**, 2004.
- 36 C. Barner-Kowollik and A. Inglis, *Macromol. Chem. Phys.*, 2009, **210**, 987–992.
- 37 T. Higashihara, K. Sugiyama, H. Yoo, M. Hayashi and A. Hirao, *Macromol. Rapid Commun.*, 2010, **31**, 1031–1059.
- 38 O. Altintas, A. L. Demirel, G. Hizal and U. Tunka, *J. Polym. Sci., Part A: Polym. Chem.*, 2008, **46**, 5916–5928.
- 39 S. Rangou and A. Avgeropoulos, *J. Polym. Sci., Part A: Polym. Chem.*, 2009, **47**, 1567–1574.
- 40 J. J. K. Kirkensgaard, *Soft Matter*, 2010, **6**, 6102–6108.
- 41 R. Groot and P. Warren, *J. Chem. Phys.*, 1997, **107**, 4423.
- 42 H. J. Limbach, A. Arnold, B. A. Mann and C. Holm, *Comput. Phys. Commun.*, 2006, **174**, 704–727.
- 43 W. Humphrey, A. Dalke and K. Schulten, *J. Mol. Graphics*, 1996, **14**, 33–38.
- 44 W. Li, Y. Xu, G. Zhang, F. Qiu, Y. Yang and A. Shi, *J. Chem. Phys.*, 2010, **133**, 064904.
- 45 S. T. Hyde, *Handbook of Applied Surface and Colloid Chemistry*, John Wiley and Sons, Ltd, 2001, ch. 16.
- 46 C.-I. Huang, H.-K. Fang and C.-H. Lin, *Phys. Rev. E: Stat., Nonlinear, Soft Matter Phys.*, 2008, **77**, 031804.
- 47 W. Pisula, X. Feng and K. Müllen, *Advanced Materials*, 2010, **XX**, 1–16.
- 48 D. A. Tomalia, *Soft Matter*, 2010, **6**, 456–474.
- 49 A. W. Bosman, H. Janssen and E. Meijer, *Chem. Rev.*, 1999, **99**, 1665–1688.
- 50 P. de Gennes and H. Hervet, *J. Phys., Lett.*, 1983, **44**, 351.
- 51 I. Chalari and N. Hadjichristidis, *J. Polym. Sci., Part A: Polym. Chem.*, 2002, **40**, 1519.
- 52 K. Orfanou, H. Iatrou, D. Lohse and N. Hadjichristidis, *Macromolecules*, 2006, **39**, 4361.
- 53 E. van Ruymbeke, K. Orfanou, M. Kapnistos, H. Iatrou, M. Pitsikalis, N. Hadjichristidis, D. Lohse and D. Vlassopoulos, *Macromolecules*, 2007, **40**, 5941.
- 54 S. Rangou, P. Theodorakis, L. Gergidis, A. Avgeropoulos, P. Efthymiopoulos, D. Smyrniaios, M. Kosmas, C. Vlahos and T. Giannopoulos, *Polymer*, 2007, **48**, 652–663.
- 55 A. Avgeropoulos, S. Rangou, V. Krikorian and E. Thomas, *Macromol. Symp.*, 2008, **267**, 16–20.
- 56 D. Lonsdale, M. Whittaker and M. Monteiro, *J. Polym. Sci., Part A: Polym. Chem.*, 2009, **47**, 6292–6303.
- 57 X. Liu and C. Zhong, *Polymer*, 2008, **49**, year.
- 58 V. Percec, B. Won, M. Peterca and P. Heiney, *J. Am. Chem. Soc.*, 2007, **129**, 11265.
- 59 V. Percec, M. Imam, M. Peterca, D. Wilson and P. Heiney, *J. Am. Chem. Soc.*, 2008, **131**, 1294.
- 60 M. Peterca, M. Imam, P. Leowanawat, B. Rosen, D. Wilson, C. J. Wilson, X. Zeng, G. Ungar, P. Heiney and V. Percec, *J. Am. Chem. Soc.*, 2010, **132**, 11288.
- 61 Y. Ding, H. Öttinger, A. Schlüter and M. Kröger, *J. Chem. Phys.*, 2007, **127**, 094904.
- 62 M. Kröger, O. Peleg, Y. Ding and Y. Rabin, *Soft Matter*, 2008, **4**, 18–28.
- 63 Y. Ding and M. Kröger, *Macromolecules*, 2009, **42**, 576–579.